ELSEVIER

Materials Science and Engineering A334 (2002) 307–311

MATERIALS SCIENCE & ENGINEERING A

www.elsevier.com/locate/msea

Glass transition and thermal stability of hard magnetic bulk NdAlFeCo metallic glass

Bing Chen Wei [a,*], Wei Hua Wang [a,b], Lei Xia [c], Zhi Zhang [b], De Qian Zhao [b], Ming Xiang Pan [b]

[a] *National Microgravity Laboratory, Institute of Mechanics, Chinese Academy of Sciences, Beijing 100080, People's Republic of China*
[b] *Institute of Physics and Center for Condensed Matter Physics, Chinese Academy of Sciences, Beijing 100080, People's Republic of China*
[c] *Institute of Materials, Shanghai University, Shanghai 200072, People's Republic of China*

Received 23 July 2001; received in revised form 24 October 2001

Abstract

Glass transition and thermal stability of bulk $Nd_{60}Al_{10}Fe_{20}Co_{10}$ metallic glass were investigated by means of dynamic mechanical thermal analysis (DMTA), differential scanning calorimetry (DSC), X-ray diffraction (XRD) and scanning electronic microscopy (SEM). The glass transition temperature, not revealed by DSC, is alternatively determined by DMTA via storage modulus E' and loss modulus E'' measurement to be 498 K at a heating rate of 0.167 K s^{-1}. The calculated reduced glass transition temperature (T_g/T_m) is 0.63. The large value of T_g/T_m of this alloy is consistent with its good glass-forming ability. The crystallization process of the metallic glass is concluded as follows: amorphous → amorphous + metastable FeNdAl phase → amorphous + primary δ-FeNdAl phase → primary δ-phase + eutectic δ-phase + Nd_3Al + Nd_3Co. The appearance of hard magnetism in this alloy is ascribed to the presence of amorphous phase with highly relaxed structure. The hard magnetism disappeared after the eutectic crystallization of the amorphous phase. © 2002 Elsevier Science B.V. All rights reserved.

Keywords: Metallic glasses; Phase transformations; Hard magnetic; Glass transition

1. Introduction

A number of new metallic alloys with excellent glass forming ability have been developed in the last 10 years, and it permits the formation of large bulky ingots of metallic glass [1–3]. These bulk metallic glasses (BMGs) have considerable potential as advanced engineering materials due to their excellent processing capabilities of the undercooled liquid, improved wear resistance, high strength, good corrosion resistance and especially soft magnetism [4–8]. More recently, NdFeAl family metallic glasses of a diameter up to 12 mm with high coercivity have been reported [9]. The NdFeAl family is a special type, because it seems to be the only family of BMGs that does not exhibit any glass transition temperature T_g prior to crystallization temperatures T_x [10]. This is anomalous because other BMGs possess a wide supercooled liquid region ($\Delta T = T_x - T_g$) [6]. Moreover, the hard magnetic properties of the glassy Nd–Fe–Al based alloys are also interesting in both scientific and practical viewpoints, as no structural anisotropy should exist in a glassy (disordered) packing of atoms. Consequently, Nd-based BMGs have received considerable attention. But most of the development has been on the magnetic properties of this novel BMGs [10–12]. There is much less information on detail study of the glass transition and crystallization process [13,14], although these processes are important in understanding the stability of these glassy materials. In this work, $Nd_{60}Al_{10}Fe_{20}Co_{10}$ BMG has been prepared by chill casting. The glass transition and thermal stability of this BMG are investigated by means of differential scanning calorimetry (DSC), dynamic mechanical thermal analysis (DMTA), X-ray diffraction (XRD) and scanning electron microscopy (SEM). The glass transition temperature and crystal-

* Corresponding author. Tel.: +86-10-8264-9198; fax: +86-10-6261-5524.
E-mail address: weibc@imech.ac.cn (B.C. Wei).

0921-5093/02/$ - see front matter © 2002 Elsevier Science B.V. All rights reserved.
PII: S0921-5093(01)01893-7

lization sequence of the BMG are determined. The result will be helpful to understand the reason for appearance of good glass forming ability and hard magnetism in Nd-based BMGs.

2. Experimental procedure

Ingots with compositions of $Nd_{60}Al_{10}Fe_{20}Co_{10}$ were prepared by arc melting from elemental Nd, Fe, Al and Co with a purity of 99.9% in a titanium-gettered argon atmosphere. Cylindrical specimens of about 3 mm in diameter and 50 mm in length were prepared from the ingots by die casting into a copper mold under argon atmosphere. The structure of the as-cast cylinder was characterized by XRD in a Siemens D5000 diffractometer using Cu K_α radiation. Thermal analysis was performed using a Perkin–Elmer DSC-7 differential scanning calorimeter under argon atmosphere. A heating rate of 0.167 K s^{-1} was applied. The dynamic mechanical properties were measured by using a dynamic mechanical thermal analyzer (DMTA IV) with three-point bending mode. In a viscoelastic solid, a sinusoidal strain is delayed from supplied sinusoidal stress by viscosity at an angle of δ. Complex modulus (E^*) is the ratio of maximum stress to maximum strain and the real and imaginary parts of E^* were defined as storage (E') and loss (E'') modulus, respectively. E' is the value of the energy which is stored and recovered perfectly during one cycle of strain change, while E'' is the loss of energy which changes to heat during one cycle. The loss tangent ($\tan\delta$) corresponds to the internal friction representing the degree of heat which was lost during one cycle. Generally, E^* is calculated by $E = |E^*| = \sqrt{E'^2 + E''^2}$. When $E' \gg E''$, the E' can be considered as E^*. In this investigation, the temperature dependence of the E', E'' and $\tan\delta$ was measured with samples of $1.2 \times 3.0 \times 30$ mm^3 in dimensions under dynamic conditions with a static load of 1 N at a frequency of 1 Hz. Microstructure was studied by a Cambridge scanning electron microscope equipped with link energy dispersive X-ray (EDX) microanalysis system. Magnetic measurements were performed using a vibrating sample magnetometer (VSM) with a maximum applied field of 1592 kA m^{-1}.

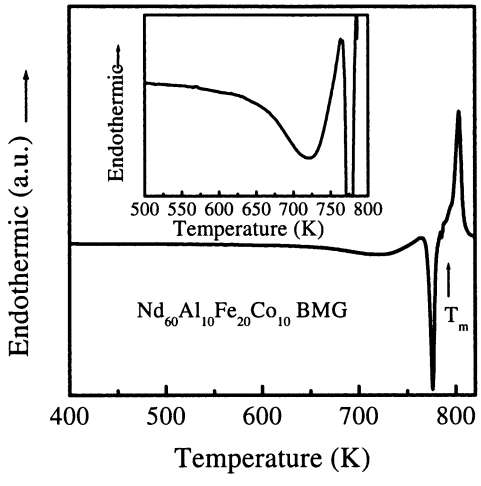

Fig. 1. DSC curve of the as-cast $Nd_{60}Al_{10}Fe_{20}Co_{10}$ BMG. The inset shows the enlarged part of the broad exothermic peak.

3. Results and discussion

The as-cast cylinder exhibits an XRD spectrum typical for amorphous phase without obvious crystalline reflection peaks. Fig. 1 shows the DSC curve of the as-cast $Nd_{60}Al_{10}Fe_{20}Co_{10}$ BMG. It exhibits two exothermic reactions, a lower temperature weak peak ranging from 642 to 754 K and a higher temperature sharp peak, followed by an endothermic reaction of melting. The obvious endothermic peak due to the glass transition is not observed in the trace, and this result is consistent with the others results on NdFeAl-based alloys [10,12]. The broad exothermic peak was also observed in previous work, but this exothermic reaction is still unclear. The sharp exothermic peak at higher temperature is caused by the marked crystallization. This also confirms the glassy structure of the as-cast sample.

Dynamic mechanical thermal analysis on the as-cast sample is shown in Fig. 2a. Starting from room temperature, initially the storage modulus E' decreases slightly as expected for conventional metals. The specimen softens markedly at 498 K, and E' decreases rapidly from 48 MPa at 498 K to 31 MPa at 588 K. Subsequently, E' shows a weak peak with an onset temperature of 588 K, and then decreases continuously with the increase of temperature. The corresponding loss modulus E'' exhibits a large loss of energy above 498 K and shows a loss peak at 571 K. The E'' curve shows the maximum value at 588 K, which corresponds to the weak peak of E' curve. The temperature dependence of $\tan\delta$ (not shown here) is similar to that of E''. E'' corresponding to the heat loss caused by a thermally activated process such as diffusion shows a rapid increase in the temperature range from 498 to 571 K, indicating that a remarkable transition occurs. In addition, the continuous increase of the E'' is accompanied by the rapid decrease of the E'. This suggests the transition is a glass transition process with a onset temperature of 498 K, which leads to the notable softening of the alloy. In order to confirm this opinion, DMTA measurement of the $Nd_{60}Al_{10}Fe_{20}Co_{10}$ BMG annealed at 538 K (above 498 K) for 1.2 ks was carried out (Fig. 2b). The significant change of E' above 498 K and E''peak similar to that of the as-cast samples is also observed. This confirms that the transition is a reversible course.

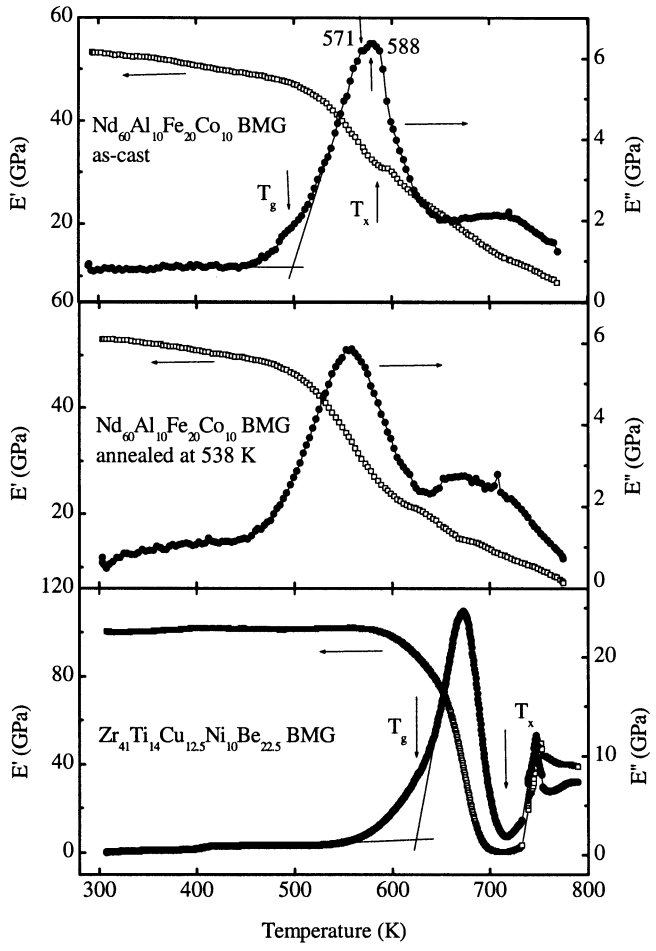

Fig. 2. Temperature dependence of storage modulus E' and loss modulus E'' of: (a) as-cast $Nd_{60}Al_{10}Fe_{20}Co_{10}$ BMG; (b) $Nd_{60}Al_{10}Fe_{20}Co_{10}$ BMG annealed at 603 K; and (c) as-cast $Zr_{41}Ti_{14}Cu_{12.5}Ni_{10}Be_{22.5}$ BMG.

Moreover, the temperature range of the E'' peak is much higher than the Curie temperature (462 K) of the BMG, so the reversible transition above 498 K is not a ferromagnetic transition. Comparative DMTA test was also conducted on $Zr_{41}Ti_{14}Cu_{12.5}Ni_{10}Be_{22.5}$ BMG with a distinct glass transition at 623 K, which is determined by DSC measurement with a heating rate of 0.167 K s^{-1}. The results are shown in Fig. 2c. It can be seen that similar rapid decrease of E' and remarkable loss of energy during glass transition were also observed. Previous studies of Chen et al. on dynamic mechanical properties of metallic glass shows that the mechanical properties decrease greatly near the glass transition temperature [15]. Anderson et al. reported that the glass transition temperatures measured by viscous flow measurement agree well with DSC results [16]. The DMTA method uses the onset of viscoelastic damping due to the rapid decrease of viscosity above T_g and is therefore based on the same property change as the viscosity measurement [17]. Depending on the above analysis, we confirm that the distinct transition of the BMG above 498 K is a glass transition.

It is worth noting that the E' value for the $Zr_{41}Ti_{14}Cu_{12.5}Ni_{10}Be_{22.5}$ sample is almost zero before crystallization, while it is still a relatively high value for the $Nd_{60}Al_{10}Fe_{20}Co_{10}$ BMG. The reason for this important difference is supposed to be that the present Nd-based BMG is a XRD amorphous, but not a fully amorphous like $Zr_{41}Ti_{14}Cu_{12.5}Ni_{10}Be_{22.5}$ BMG. In fact, a large number of nano-scaled crystals, not resolved by XRD, but have been observed by transition electronic microscopy (TEM) in the as-cast Nd–Fe based BMGs and even in melt-spinning ribbons [10,12]. The presence of these nano-crystals greatly increases the viscosity and modulus of the supercooled liquid. It must be pointed out that the notable glass transition exhibited in the DMTA results is not observed in the DSC curve in the same temperature range. The reason for this very weak thermal effect is probably that the glass transition takes place rather gradually in Nd–Fe system due to the presence of a wide distribution of the composition in the amorphous phase. This is supported by the recent study of the magnetization–temperature relationship in Nd–Fe based BMG, in which a rather broad and clear magnetic transition was observed from 10 to 80 K, suggesting the probably presence of amorphous phase with a wide composition range [18].

The weak peak of E' value in Fig. 2a at 588 K and the corresponding sharp E'' peak of the as-cast sample indicate that certain crystallization reaction occurs at this temperature, and causes the sudden increase of the viscosity of the supercooled liquid. The E' peak and loss energy peak due to crystallization are also observed in the DMTA curves of $Zr_{41}Ti_{14}Cu_{12.5}Ni_{10}Be_{22.5}$ BMG as shown in Fig. 2c. However, the magnitude of the increase of E' due to crystallization in $Nd_{60}Al_{10}Fe_{20}Co_{10}$ BMG is much smaller than that in $Zr_{41}Ti_{14}Cu_{12.5}Ni_{10}Be_{22.5}$ BMG (Fig. 2c). It can be inferred that the volume fraction of the crystalline phase precipitated at around 588 K has quite a small value. In the temperature range from 642 to 754 K, the E'' curve in Fig. 2a shows a broad peak, which corresponds to the broad exothermal reaction in DSC curve in same temperature range (Fig. 1). This means that certain phase transition occurs, and this phase transition does not significantly change the E' value of the BMG as shown in Fig. 2a.

The XRD results of the isothermal annealed $Nd_{60}Al_{10}Fe_{20}Co_{10}$ are shown in Fig. 3. Annealing at 643 K for 1.8 ks results in the appearance of unknown metastable phases, which transform into an equilibrium phase after annealing at 723 K. The back scattering electron (BSE) image shows that no obvious compositional contrast is seen in the as-cast sample (Fig. 4a). The unknown metastable phases in the sample annealed at 643 K are dark, rod-like granules with a Fe:Nd:Al ratio of 75:16:9 as shown in Fig. 4b. The volume

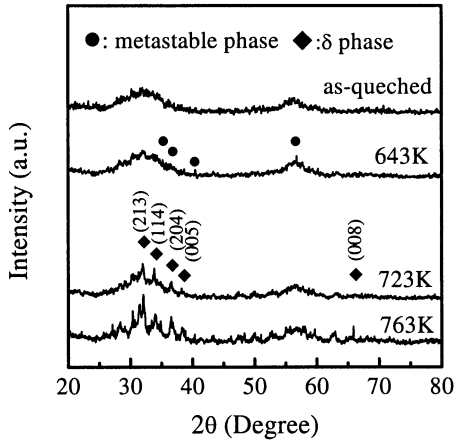

Fig. 3. Results of XRD for $Nd_{60}Al_{10}Fe_{20}Co_{10}$ annealed at different temperatures for 1.8 ks.

fraction of the metastable phase is estimated to be about 8.2% by calculating the difference of the crystallization enthalpy between as-cast sample and the sample annealed at 643 K for 1800 s. This result suggests that the weak E' peak at 588 K in Fig. 2a is caused by the precipitation of metastable FeNdAl phase, which is not resolved by the DSC measurement due to its small quantity. The structure of this metastable FeNdAl ternary phase is under investigation. After annealing at 723 K, the BSE results show that, the rod-like metastable phase is disappeared. Instead, a plate-like stable phase distributes in the remaining amorphous matrix as shown in Fig. 4c. The EDX results show that, this phase contains less Fe, and its Fe:Nd:Al ratio is 49:34:17. This composition is close to the composition range of the δ-phase ($Fe_{67.5-x}Al_xNd_{32.5}$, $7 < x < 25$), which is hexagonal with antiferromagnetism [19–21]. The XRD and SEM results show that the broad peak in the loss modulus and DSC curves in the temperature range from 642 to 754 K is caused by the transition from metastable FeNdAl phase to primary δ-FeNdAl ternary phase. The BSE image of the $Nd_{60}Al_{10}Fe_{20}Co_{10}$ annealed at 763 K show that the structure consists of primary δ plus eutectic phases as shown in Fig. 4d. The EDX results show the eutectic consists of the thin plate-like eutectic δ, dark Nd_3Al, and bright Nd_3Co. This structure is similar to the ternary NdAlFe eutectic [19,20]. This result means that the sharp exothermic peak in the DSC trace is attributed to eutectic crystallization of the remaining amorphous.

According to the above results, the reduced glass transition temperature T_{rg}, termed as the ratio between T_g and melting point T_m, of the studied alloy is calculated to be 0.63, and the supercooled liquid region ΔT is 90 K. The large value of T_{rg} and ΔT of this alloy is in consistent with its good glass-forming ability.

The dependence of H_c, M_s and M_r on isothermal annealing temperature for $Nd_{60}Al_{10}Fe_{20}Co_{10}$ alloy is shown in Fig. 5. The results show that the as-cast $Nd_{60}Al_{10}Fe_{20}Co_{10}$ BMG exhibits hard magnetic behavior with a coercivity of 326 kA m^{-1}. The hard magnetic properties remain almost unchanged in the annealing temperature range up to 743 K below the eutectic crystallization temperature determined by above analysis. This indicates that the precipitation and growth of the unknown metastable FeNdAl phase and the primary δ-FeNdAl phase did not greatly change the magnetic properties of $Nd_{60}Al_{10}Fe_{20}Co_{10}$ glass, and the completely crystallization results in the disappearing of hard magnetic properties. It has been reported that a metastable Nd_5Fe_{17} phase was responsible for the high coercivity in melt-spun binary Nd–Fe ribbons [22]. However, this phase was not found in our samples. The δ-phase is antiferromagnetic with a Neel temperature of approximately 260 K [19,21]. The magnetic properties

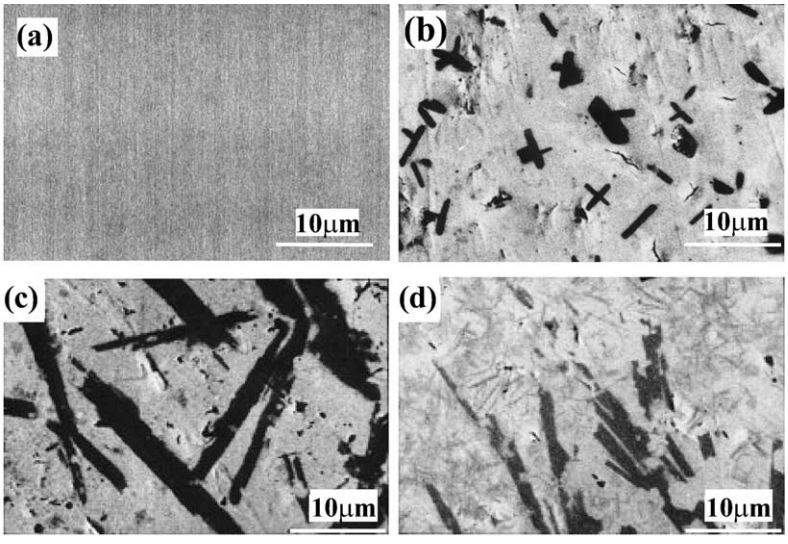

Fig. 4. BSE images of $Nd_{60}Al_{10}Fe_{20}Co_{10}$ annealed at different temperatures for 1.8 ks: (a) as-cast; (b) 643 K; (c) 723 K; and (d) 763 K.

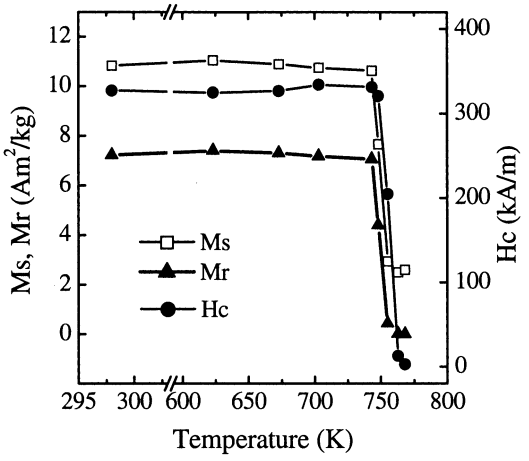

Fig. 5. Dependence of H_c, M_s and M_r on isothermal annealing temperature for $Nd_{60}Al_{10}Fe_{20}Co_{10}$ alloy (annealing for 1.8 ks).

of the metastable FeNdAl are thought to be antiferremagnetic or paramagnetic. These indicate that the high coercivity in the NdAlFeCo alloy is due to the presence of the amorphous phase. Our results support the previously proposed ferromagnetic cluster model with large random anisotropy, and it shows that the high coercivity is attributed to the development of the homogeneous dispersion of the Fe(Co)-rich clusters with large local magnetic anisotropy from the highly relaxed disordered structure developed at a cooling rate of about 10^1–10^2 K s^{-1}, which is much slower than the cooling rate of 10^4–10^6 K s^{-1} in conventional spun-melt method [23]. No distinct low temperature relaxation transition is found in both DSC and DMTA curves of the as-cast sample, and it confirms the relaxed structure of $Nd_{60}Al_{10}Fe_{20}Co_{10}$ BMG.

4. Conclusions

In conclusion, the glass transition temperature of $Nd_{60}Al_{10}Fe_{20}Co_{10}$ BMG is determined by DMTA to be around 498 K at heating rate of 0.167 K s^{-1}. The calculated T_g/T_m shows a high value of 0.63, which is consistent with the good glass-forming ability of this alloy. The crystallization process of this BMG is concluded as follows: amorphous → amorphous + metastable FeNdAl phase → amorphous + primary δ-FeNdAl phase → primary δ-phase + eutectic δ-phase + Nd_3Al + Nd_3Co. The precipitation and growth of the metastable FeNdAl and the primary δ-phase have no significant effect on the magnetic properties of the $Nd_{60}Al_{10}Fe_{20}Co_{10}$ glass.

Acknowledgements

The authors are grateful to the financial support of the National Natural Science Foundation of China (grant No. 50101012 and 59925101).

References

[1] A. Inoue, T. Zhang, T. Masumoto, Mater. Trans. JIM 31 (1990) 425.
[2] A. Inoue, T. Zhang, N. Nishiyama, K. Ohba, T. Masumoto, Mater. Trans. JIM 33 (1992) 937.
[3] A. Peker, W.L. Johnson, Appl. Phys. Lett. 63 (1993) 2342.
[4] W.L. Johnson, Mater. Sci. Forum 225–227 (1996) 35.
[5] T.G. Nieh, T. Mukai, C.T. Liu, J. Wadsworth, Scripta Mater. 40 (1999) 1021.
[6] A. Inoue, Acta Mater. 48 (2000) 279.
[7] A. Inoue, T. Zhang, A. Takeuchi, Appl. Phys. Lett. 71 (1997) 58.
[8] W.H. Wang, Q. Wei, M.P. Macht, S. Friedrich, H. Wollenberger, Appl. Phys. Lett. 71 (1997) 1053.
[9] A. Inoue, T. Zhang, A. Takeuchi, W. Zhang, Mater. Trans. JIM 37 (1996) 636.
[10] A. Inoue, A. Takeuchi, T. Zhang, Metall. Mater Trans. 29A (1998) 1779.
[11] G.J. Fan, W. Loser, S. Roth, J. Eckert, L. Schultz, Appl. Phys. Lett. 75 (1999) 2984.
[12] X.Z. Wang, Y. Li, J. Ding, L. Si, H.Z. Kong, J. Alloys Compd. 290 (1999) 209.
[13] Y. Li, S.C. Ng, Z.P. Lu, Y.P. Feng, K. Lu, Philos. Mag. Lett. 78 (1998) 213.
[14] B.C. Wei, Y. Zhang, Y.X. Zhuang, D.Q. Zhao, M.X. Pan, W.H. Wang, W.R. Hu, J. Appl. Phys. 89 (2001) 3529.
[15] H.S. Chen, N. Morito, J. Non-Cryst. Solids 72 (1985) 287.
[16] P.M. Anderson III, A.E. Lord Jr., Mater. Sci. Eng. 43 (1980) 267.
[17] R. Rambousky, M. Moske, K. Samwer, Mater. Sci. Forum 179–181 (1995) 761.
[18] R.J. Ortega-Hertogs, A. Inoue, K.V. Rao, Scripta Mater. 44 (2001) 1333.
[19] B. Grieb, E.-Th. Henig, G. Martinek, H.H. Stadelmaier, G. Petzow, IEEE Trans. Magn. 26 (1990) 1367.
[20] V. Pierre, Handbook of Ternary Alloy Phase Diagrams, ASM International, Materials Park, OH, 1994, p. 3525 and 3052.
[21] J. Ding, L. Si, Y. Li, X.Z. Wang, Appl. Phys. Lett. 75 (1999) 1763.
[22] H.H. Stadelmaier, G. Schneider, E. Henig, M. Ellner, Mater. Lett. 10 (1991) 303.
[23] K. Nagayama, H. Ino, N. Sato, Y. Nakagawa, E. Kita, K. Siratori, J. Phys. Soc. Jpn. 59 (1990) 2483.